

Global Measurements of Brown Carbon and Estimated Direct Radiative Effects

Rodney J. Weber¹, Linghan Zeng², Aoxing Zhang², Yuhang Wang², Nicholas L. Wagner³, Joseph M. Katich⁴, Joshua Peter Schwarz⁴, Gregory P. Schill⁵, Charles A. Brock⁴, Karl Froyd⁶, Daniel M. Murphy⁴, Christina Williamson⁴, Agnieszka Kupc⁷, Eric Scheuer⁸, and Jack E. Dibb⁹

¹Georgia Institute Of technology

²Georgia Institute of Technology

³NOAA/ESRL/CSD

⁴NOAA Earth System Research Laboratory

⁵Earth System Research Laboratory

⁶National Oceanic and Atmospheric Administration (NOAA)

⁷NOAA ESRL

⁸University of New Hampshire-Durham

⁹University of New Hampshire

November 21, 2022

Abstract

Brown carbon (BrC) is an organic aerosol material that preferentially absorbs light of shorter wavelengths. Global-scale radiative impacts of BrC have been difficult to assess due to the lack of BrC observational data. To address this, aerosol filters were continuously collected with near pole-to-pole latitudinal coverage over the Pacific and Atlantic basins in three seasons as part of the Atmospheric Tomography Mission. BrC chromophores in filter extracts were measured. We find that globally, BrC was highly spatially heterogeneous, mostly detected in air masses that had been transported from regions of extensive biomass burning. We calculate the average direct radiative effect due to BrC absorption accounted for approximately 7 to 48% of the top of the atmosphere clear sky instantaneous forcing by all absorbing carbonaceous aerosols in the remote atmosphere, indicating that BrC from biomass burning is an important component of the global radiative balance.

Hosted file

zhang atom grl agusupporting-information_word_template.docx available at <https://authorea.com/users/528434/articles/596870-global-measurements-of-brown-carbon-and-estimated-direct-radiative-effects>

1 **Global Measurements of Brown Carbon and Estimated Direct** 2 **Radiative Effects**

3 Linghan Zeng¹, Aoxing Zhang¹, Yuhang Wang¹, Nicholas L. Wagner^{2,3}, Joseph M. Katich^{2,3}, Joshua P.
4 Schwarz³, Gregory P. Schill^{2,3}, Charles Brock³, Karl D. Froyd^{2,3}, Daniel M. Murphy³, Christina J Williamson^{2,3},
5 Agnieszka Kupc^{3,4}, Eric Scheuer⁵, Jack Dibb⁵, Rodney J. Weber¹

6
7 ¹School of Earth and Atmospheric Sciences, Georgia Institute of Technology, Atlanta, GA 30332, USA

8 ²Cooperative Institute for Research in Environmental Sciences, University of Colorado, Boulder, CO 80309,
9 USA

10 ³Chemical Sciences Laboratory, National Oceanic and Atmospheric Administration, Boulder, CO 80305, USA

11 ⁴Faculty of Physics, University of Vienna, Vienna, Austria

12 ⁵Institute for the Study of Earth, Oceans, and Space, University of New Hampshire, Durham, NH 03824, USA

13

14 *Correspondence to:* Rodney J. Weber (rweber@eas.gatech.edu)

15

16

17 **Key Points:**

18

19 • Globally, biomass burning is a large source of light absorbing carbonaceous aerosol that directly affect

20 the planetary radiation balance.

21

22 • Transported over long distances, brown carbon is a significant component of these aerosols, but its

23 contribution was highly variable.

24

25 • For these data, brown carbon contributed up to 48% to the top of the atmosphere average clear sky

26 instantaneous forcing by light absorption by carbonaceous aerosols.

27

28

29

30 Abstract

31 Brown carbon (BrC) is an organic aerosol material that preferentially absorbs light of shorter wavelengths.
32 Global-scale radiative impacts of BrC have been difficult to assess due to the lack of BrC observational data. To
33 address this, aerosol filters were continuously collected with near pole-to-pole latitudinal coverage over the
34 Pacific and Atlantic basins in three seasons as part of the Atmospheric Tomography Mission. BrC
35 chromophores in filter extracts were measured. We find that globally, BrC was highly spatially heterogeneous,
36 mostly detected in air masses that had been transported from regions of extensive biomass burning. We calculate
37 the average direct radiative effect due to BrC absorption accounted for approximately 7 to 48% of the top of the
38 atmosphere clear sky instantaneous forcing by all absorbing carbonaceous aerosols in the remote atmosphere,
39 indicating that BrC from biomass burning is an important component of the global radiative balance.

40

41 Plain Language Summary

42

43 Combustion produces light absorbing aerosols that can affect the global radiation balance. Black carbon, which
44 absorbs light over a broad wavelength range, has been extensively studied, but recent work shows that a
45 significant component of the light absorbing aerosol is brown, absorbing mostly in the lower end of the visible
46 and into the UV. Incomplete combustion, such as in wild fires, is known to produce substantial levels of brown
47 carbon. Here we report direct measurements of brown carbon determined from filter samples collected from
48 aircraft flights that extended from pole to pole over three seasons. We observed brown carbon in aerosols that
49 had been transported long distances from regions of wild fires at various locations across the globe. A radiative
50 transfer model indicated that this brown carbon can substantially contribute to the overall radiative forcing by
51 light absorbing aerosols.

52

53 1 Introduction

54 Atmospheric aerosols affect the global radiative balance by scattering and absorbing radiation [*Chýlek and*
55 *Coakley, 1974*]. The main light absorbing component of aerosols is black carbon (BC) [*Bond and Bergstrom,*
56 *2006; Horvath, 1993*], however, some components of mineral dust [*Sokolik and Toon, 1999*] and organic
57 aerosols (OA) also absorb visible light. Organic chromophores in aerosol particles are the least well understood

58 and are overall referred to as brown carbon (BrC) because they absorb most strongly in the UV and near-visible
59 wavelengths, resulting in a brownish or yellow appearance.

60

61 One known major source for BrC are products of incomplete combustion of fossil and biomass fuels [*Chen and*
62 *Bond, 2010; Desyaterik et al., 2013; Hecobian et al., 2010; Hoffer et al., 2006; X Zhang et al., 2013*]. The
63 complex molecular structures of organic chromophores are challenging to exactly determine, although nitro-
64 aromatic compounds have been identified in urban and biomass burning aerosols [*Claeys et al., 2012; P Lin et*
65 *al., 2016*]. Other compounds, such as polycyclic aromatic hydrocarbon derivatives and polyphenols may
66 contribute to aerosol light absorption properties as well [*P Lin et al., 2016*]. Field observations of wildfires in
67 California [*Forrister et al., 2015*], the Amazon [*Wang et al., 2016*], and Crete [*Wong et al., 2019*] have
68 indicated that a large fraction of emitted BrC can be depleted over time by bleaching, with a half-life varying
69 between 9 and 24 hours. However, studies show a small fraction of emitted chromophores of high molecular
70 weight resist bleaching. Low molecular weight chromophores that rapidly bleach would then mainly contribute
71 to BrC absorption near sources, while high molecular weight chromophores with longer lifetimes could continue
72 to contribute to light absorption in aged biomass burning plumes over large spatial scales [*Di Lorenzo and*
73 *Young, 2016; Wong et al., 2017*].

74

75 Estimation of the global aerosol direct radiative effects in past studies treated OA as wholly non-absorbing
76 [*Bellouin et al., 2005; Haywood and Boucher, 2000*], whereas a variety of recent studies have attempted to
77 estimate the global radiative impact of BrC. These studies are limited by incomplete knowledge of BrC sources,
78 sinks, evolution, and chemical composition-driven optical properties, and there is little data to assess model
79 predictions. They estimate that the global average top of atmosphere (TOA) BrC direct radiative effect (DRE),
80 which is its instantaneous radiative impact on the Earth's energy balance [*Heald et al., 2014*], ranges from +0.04
81 to +0.57 W m⁻², with BrC contributing from 20 to 40% of DRE from total carbonaceous absorbing aerosol (i.e.,
82 BC+BrC) [*Feng et al., 2013; Jo et al., 2016; G Lin et al., 2014; Saleh et al., 2015*]. These model simulations
83 depend on parameterized BrC emissions, often based on the BC-to-OA ratio, or modified combustion efficiency
84 (MCE) [*Jo et al., 2016; Saleh et al., 2014*]. They also assumed an invariant (non-bleaching) BrC following
85 emission. In contrast, *Wang et al. [2018]* included BrC bleaching utilizing a one-day photochemical lifetime and
86 predicted a global BrC DRE of +0.048 W m⁻² and a similar BrC contribution to DRE by all carbonaceous
87 aerosol absorption (23%). Other modeling studies that included both bleaching and the added effect of BrC
88 enhancement relative to BC with increasing altitude [*Y Zhang et al., 2017*], found that DRE due to upper

89 troposphere BrC can largely offset BrC bleaching [A Zhang *et al.*, 2020]. Model skill has often been assessed
90 by comparison with BrC inferred from AERONET data, but this data has substantial uncertainty itself [Schuster
91 *et al.*, 2016]. Global-scale data sets of measured BrC are needed for evaluation of model predictions and an
92 assessment of its importance on the radiative balance. Here, the first estimates of BrC DRE and importance
93 relative to BC, based on direct observational data over large spatial scales, is reported.

94 **2 Method**

95 **2.1 The ATom Mission (Atmospheric Tomography Mission)**

96 The NASA DC-8 aircraft conducted research flights nearly pole to pole along the central Pacific (north to south)
97 and Atlantic (south to north) Oceans at altitudes systematically alternating from near surface (180 m) to ~13 km
98 above sea level over four deployments, one in each season (see Table 1), [Prather *et al.*, 2017]. A map is shown
99 in Figure 1. (BrC measurements were made in ATom-2, 3, and 4 deployments).

100 **2.2 Filter Sampling, Extraction and Analysis**

101 The particle filter sampling system and offline analysis was identical to that used in two previous studies on the
102 DC-8, SEAC⁴RS and DC3 and the method described in those publications [Forrister *et al.*, 2015; Liu *et al.*,
103 2015; Liu *et al.*, 2014; Y Zhang *et al.*, 2017]. Particles with aerodynamic diameter less than nominally 4.1 μm
104 [McNaughton *et al.*, 2007] were collected onto Teflon filters over all altitudes at intervals typically <5 minutes
105 at altitudes below 3 km and a maximum of 15 minutes for higher altitudes. For all three missions, 1074 filters
106 were collected and analyzed, including two or three blank filters per flight. Only results from water extractions
107 are reported here due to high blanks in methanol extractions. Light absorption spectra of the extract was
108 measured with a spectrophotometer utilizing a 2.5 m long liquid waveguide. A schematic of the method is
109 shown in Supplemental Information Figure S1, along with a more detailed description of the method. Light
110 absorption coefficient of chromophores in solution was calculated following Hecobian *et al.* [2010]. In the
111 following, the absorption coefficient averaged between 360 and 370 nm (avg. 365 nm) was used as a measure of
112 particle BrC levels (i.e., $\text{BrC} = \text{Abs}_{365\text{nm}}$). BrC Absorption Ångström Exponents (AAE; $\text{Abs}_\lambda = C \cdot \lambda^{-\text{AAE}}$)
113 were also determined from the measured spectra (see Figure S2 for example spectra). Note that all data
114 presented here are at standard temperature and pressure (273K & 1013 mb), however, these are converted to
115 ambient conditions for the radiative calculations discussed below.

116

117 Limit of detection (LOD) was determined by three times the standard deviation of field blank filters, combining
118 all blanks from a given deployment (Table 1). (See also Figure S3 for frequency distribution of all water-soluble
119 BrC data relative to calculated LODs for each mission). In the following analysis we focus on only water-
120 soluble BrC (WS BrC) due to high blanks associated with methanol extractions. BrC measurement uncertainty
121 was calculated by propagating the uncertainties from sample collection to data analysis and is estimated at 20%,
122 where the uncertainty associated with subtracting the blank contributed 40 to 60% of this overall estimate.

123

124 The light absorption measured in this study are largely by individual chromophores (molecules) dissolved in
125 solution, not the absorption of suspended particulate. This technique was used since it exclusively measures BrC
126 optical properties (BC is not included), resulting in a highly sensitive approach required for this remote
127 atmosphere study, however when used for analysis of filters, the main limitation is blank variability, as noted
128 above. Past studies, based on measured BrC aerosol size distributions and Mie theory, indicate that a
129 multiplication factor of 1.8 to 2.1 (roughly 2 ± 0.2 , or $\pm 10\%$) can be used to estimate the light absorption by
130 aerosol particles based on measurements of chromophores in the bulk liquid extracts [Liu *et al.*, 2013; Shetty *et*
131 *al.*, 2019; Washenfelder *et al.*, 2015; Y Zhang *et al.*, 2017]. We include this in the subsequent overall uncertainty
132 analysis, which is discussed more below.

133 **2.3 Other Measurements on the DC-8, Back Trajectories and Fire Events**

134 Refractory black carbon (rBC, or just BC here) content of individual particles was measured with a single
135 particle soot photometer (SP2). Integrated BC concentrations have been adjusted to account for accumulation-
136 mode BC outside of the SP2's detection size range [Schwarz *et al.*, 2008], and in-cloud measurements were
137 removed based on cloud-probe data. In the following analysis, solvent-extracted BrC and SP2 BC are assumed
138 to encompass all absorbing carbonaceous aerosols. Methanol has been shown to extract greater than 92% of BrC
139 from laboratory-generated smoke [Chen and Bond, 2010], but other forms of light absorbing aerosols from wild
140 fires may not be included in BrC by solvent extraction [Shetty *et al.*, 2019], nor SP2 BC measurements, which
141 would lead to our under-measuring carbonaceous aerosol absorption in this study [Adler *et al.*, 2019]. Aerosol
142 scattering was derived from particle number size distributions for dry sizes between 2.7 nm to 4.8 μm in
143 diameter which were measured at 1 Hz using a suite of particle counters [Brock *et al.*, 2019]. The NOAA
144 Particle Analysis by Laser Mass Spectrometry (PALMS) instrument was used to assess both the relative
145 contributions and mass concentrations of biomass burning sources to the ambient aerosol that encompasses
146 particles of sizes between 0.1 and 4.8 μm [Froyd *et al.*, 2019; Schill *et al.*, 2020].

147

148 Airmass 72 hr back trajectories were computed using the Hybrid Single-Particle Lagrangian Integrated
149 Trajectory (HYSPLIT) analysis method [Rolph *et al.*, 2017; Stein *et al.*, 2015]. Locations and fire radiative
150 power (FRP) of large biomass burning regions for each ATom deployment were obtained from the Fire
151 Information for Resource Management System (FIRMS, <https://firms.modaps.eosdis.nasa.gov/map/>). Fires of
152 FRP greater than 100 MW are only included in the analysis. Air mass transport time from fire emissions to the
153 point of aircraft sampling was estimated based on HYSPLIT back trajectories from the sampling location to the
154 nearest FIRMS-identified wildfire intersected by the trajectory. Type of fuel, or other variables that may affect
155 emissions, were not considered. More details are provided in the Supplemental Information.

156 **2.4 Radiative Impact of BrC**

157 Radiative transfer calculations were performed with the Santa Barbara DISORT Atmospheric Radiative
158 Transfer (SBDART) model [Ricchiuzzi *et al.*, 1998] to compute the direct short-wave (0.25-4 μm) radiative
159 effect at the top of the atmosphere (TOA). Accuracy of the model is discussed by Obregón *et al.* [2015] and
160 more details are described in Y Zhang *et al.* [2017]. Estimates of aerosol scattering from dry aerosol size
161 distributions, and measurements of BC and BrC collected during aircraft vertical profiling were used in the
162 calculations. In-cloud data were excluded. Either for a complete ATom mission, or for a given geographical
163 region, all vertical profile data were averaged (mean) and then used in the radiative calculation. The aerosol
164 scattering coefficient (b_{scat}) was calculated at multiple wavelengths from the measured dry (usually < 20% RH)
165 size distribution spanning particle diameters of 2.7 nm to 4.8 μm . All aerosols were assumed to be solely
166 composed of ammonium sulfate (refractive index of 1.52+0i) [Brock *et al.*, 2019], and then ambient size
167 estimated based on temperature, pressure and RH to obtain the overall ambient scattering coefficient. Data were
168 fitted with a power law ($b_{scat} = A \cdot \lambda^{-SAE}$, A is a constant and SAE is the scattering Ångström exponent), which
169 was then used with light scattering data to determine the aerosol scattering over all wavelengths in the radiative
170 forcing calculation. The light absorption coefficient for BC (b_{BC}) was calculated from the measured BC mass
171 concentration using a mass absorption cross-section (MAC) of 10.0 m^2/g at 660 nm and AAE of 1 to compute
172 absorption at other wavelengths. This is equivalent to a factor of 1.6 lensing effect due to BC coatings (i.e., for
173 uncoated BC a MAC of 6.25 m^2/g at 660 nm is typically used) [Y Zhang *et al.*, 2017]. If BC absorption is
174 actually larger than this due to greater lensing effects, or AAEs > 1, we will overestimate the BrC contribution
175 to radiative forcing. For BrC, measured absorption at 365 nm ($\text{Abs}_{365\text{nm}}$) and an AAE value of 5 (the average of
176 the measured WS BrC AAE, discussed below), was used to compute absorption at all wavelengths (b_{BrC}).

177

178 The water-soluble light absorption data were converted to an overall aerosol BrC absorption coefficient by the
179 combination of two factors. First, the factor to convert water-soluble BrC to total BrC in solution. Based on our
180 data (Table 1), the ratio of WS BrC to total BrC for all ATom data is $53\% \pm 17\%$. Other studies have reported
181 the WS BrC to total BrC ratio for aged aerosols to be in the range of 25% to 80% [Chen and Bond, 2010; Liu et
182 al., 2015; Phillips and Smith, 2017; Satish and Rastogi, 2019; Shetty et al., 2019; Wong et al., 2017; X Zhang et
183 al., 2013]. Here we assume the ratio is 0.5 with $\pm 40\%$ uncertainty, meaning the WS BrC is multiplied by 2
184 ($\pm 40\%$ uncertainty) to estimate the contribution of all chromophores to BrC. We then convert the chromophores
185 absorption to an aerosol light absorption coefficient. This factor depends on the particle size distribution of BrC,
186 which, as discussed above is, estimated to be a factor of 2 ± 0.2 (10%), meaning the overall conversion factor is
187 4. More recent simultaneous measurements in smoke plumes of aerosol absorption with a photoacoustic
188 instrument and the same BrC filter sampling system utilized here show an overall conversion ratio of 3.21
189 ($r^2=0.84$) for WS BrC to aerosol absorption at a wavelength of 405 nm, consistent with the factor of 4 here,
190 considering uncertainty (see Figure S4). Including the uncertainty in BrC measurement of 20% (discussed
191 above), we estimate the overall BrC aerosol light absorption coefficient determined by this method has an
192 uncertainty of $\pm 46\%$.

193

194 To parse out the various aerosol contributions to TOA radiative effects, we performed 3 SBDART runs to
195 determine: (1) DRE due to only scattering; (2) DRE due to scattering and BC absorption; (3) DRE due to
196 scattering, BC absorption and BrC absorption. We estimated the DRE of BC by subtracting (1) from (2), and the
197 DRE of BrC by subtracting (2) from (3). More model details are provided in the Supplementary Information.

198 **3 Results and Discussion**

199 **3.1 Global Distribution of Fires and BrC**

200 BrC measured in ATom-2, 3 and 4 is shown in Figure 1, along with air mass back trajectories for those regions
201 where WS BrC was above the LOD. Locations of burning are shown with indicated fire radiative power (FRP),
202 for fires with FRP >100 MW. We find that WS BrC was very low over vast areas (also see Table 1), however,
203 there were regions of significant WS BrC; these include the mid-Atlantic Ocean, northern Pacific Ocean, and
204 southern Pacific Ocean near islands in Oceania (Australia, New Zealand, etc.).

205

206 In the tropical or mid-Atlantic region, enhanced levels of WS BrC were recorded in all three missions. FIRMS-
207 identified wildfires and back trajectories suggest that the BrC source for this region was either fires in South
208 America or Africa. In ATom-2 (Jan.-Feb.), most fires were in equatorial regions in northern South America and
209 Africa, coinciding with the dry period for these regions (Jan.-Apr.). These measurements accounted for a
210 majority of the observed BrC above LOD for the complete ATom-2 mission. During ATom-3 (Sept.-Oct.), the
211 fires in South America were found further south, following the movement of dryer regions southward, dictated
212 by the annual movement of the Inter-Tropical Convergence Zone. Compared to ATom-2, the wildfires were also
213 more extensive in ATom-3 in terms of both fire density and radiative power (FRP). In the last mission, ATom-4
214 (Apr.-May), the extent of fires in these regions decreased to the lowest levels relative to the ATom-2 and 3
215 missions. Levels of BrC recorded in the mid-Atlantic tracked these seasonal trends.

216

217 For the North Pacific Basin in Figure 1, WS BrC was observed in ATom-3 and 4 and back trajectories indicated
218 that the BrC was from northeastern China, but occasionally from fires in western North America. Nearly no WS
219 BrC was above the LOD in ATom-2 in this region, which could be due to differences in emissions and transport
220 with season. BrC from biofuels or other forms of incomplete combustion may also contribute, but would not be
221 evident from the FRP data. For the tropical mid-Pacific Ocean (Figure 1), BrC above LOD was only observed in
222 ATom-3 and 4, possibly from scattered islands in the region, such as Hawaii. In the south Pacific, BrC was
223 observed downwind of Indonesia, Australia and New Zealand (Oceania), mainly during ATom-3, suggesting it
224 was also highly seasonal. For example, the Oceania region fire counts with FRP greater than 100 MW during
225 ATom-2 was 419, while there were 6721 and 3749 counts during ATom-3 and 4, respectively. BrC was
226 occasionally above LOD when sampling near or within polar regions (Antarctic and Arctic) during ATom-3 and
227 4, where back trajectories show the air masses were mainly from high latitude regions, although it was difficult
228 to locate specific sources for this region. BrC in polar regions may persist longer due to low sunlight limiting
229 BrC photochemical bleaching.

230

231 As can be seen in Figure 1, the number of fire events identified from FIRMS varied significantly with region
232 and season (i.e., ATom deployment). In general, trends of fire counts and levels of WS BrC were similar;
233 highest fire counts were mainly seen in ATom-3 and highest BrC levels were generally recorded in that mission
234 (Table 1). However, significant scatter in this relationship can be expected since the aircraft did not necessarily
235 sample plumes from all fires identified by FIRMS and there are uncertainties in both WS BrC and fire events
236 identified by MODIS [Schroeder *et al.*, 2008]. Overall, we conclude that biomass burning appears to be the

237 predominant source for BrC in the remote atmosphere since most regions of recorded BrC could be traced to a
238 burning region. (We also found regions where measured $\text{BrC} < \text{LOD}$ did not intercepted burning regions, see
239 Figure S5). Given that the smoke plumes were transported over great distances ($>10,000$ km), some portion of
240 the fire-emitted BrC persisted for at least 3 days, the limit of our back trajectory analysis, consistent with
241 laboratory studies that high molecular weight BrC species resist photobleaching.

242 3.2 BrC Correlation with BC

243 Correlations provide further evidence that the BrC was associated with mainly biomass burning. Biomass
244 burning emits BC and BrC, although there are differences in emissions rates depending on fuel and burning
245 temperature, and how these species may be altered with atmospheric age. More BrC is emitted per fuel burned
246 in smoldering compared to flaming fires [Chakrabarty *et al.*, 2016], whereas more BC is emitted in flaming than
247 smoldering [Echalar *et al.*, 1995]. Some fraction of BrC will bleach over time, whereas BC is chemically stable,
248 and only undergoes removal from the air with an estimated lifetime of about <5 to 10 days globally [Cooke and
249 Wilson, 1996; Koch *et al.*, 2009; Lund *et al.*, 2018]. Also, there is evidence that BrC is lofted to higher altitudes
250 by convection more efficiently than BC [Y Zhang *et al.*, 2017], thus some scatter between BrC and BC is
251 expected even if both are emitted from wild fires in a given region. The Pearson correlation (r) between BrC and
252 BC was 0.86, 0.75 and 0.53 for ATom-2, 3 and 4, respectively (for scatter plots, see supplemental material
253 Figure S6, also see Table S1). Despite high correlations, there is significant variability at lower levels,
254 suggesting that BC cannot solely be used to infer BrC optical effects. Data with moderate to low WS BrC, but
255 very low BC, were mostly observed at higher altitudes (>9 km), possibly due to differences in advection of these
256 species through clouds [Y Zhang *et al.*, 2017], whereas periods (filter samples), that contained moderate to low
257 BC, but very low WS BrC were mainly found in the mid-Atlantic Ocean region. Causes may be different
258 burning conditions (smoldering/flaming) and processing during transport.

259

260 Comparing amongst separate ATom missions, the highest correlations between BrC and BC was found in
261 ATom-2 (0.86); the correlations were weaker in ATom-3 (0.75) and lowest in ATom-4 (0.53). A similar,
262 although somewhat stronger correlation trend was found for BrC vs. estimated biomass burning potassium
263 (K^+_{BB}), and between K^+_{BB} vs. BC (see Table S1 and supplemental material discussion for calculation of K^+_{BB}).
264 The trend was also seen in BrC and the PALMS estimate of biomass burning particle mass (See Figure S6). A
265 possible explanation is BrC observed in ATom-2 was mainly from two concentrated regions of burning (see
266 Figure 1a), whereas in ATom-3 and 4, data were from fires located in differing geographic regions. Thus,

267 although the total impact of fires may be higher for ATom-3 and 4, the characteristics of the emissions and
268 effects during transport might be broader and more complex, which weakened the correlations.

269 **3.3 Direct Radiative Effect of BrC Aerosol**

270 Light absorption over the full spectral wavelength range is necessary to simulate the radiative impact of BrC
271 aerosol. As noted in the Methods, we use a constant BrC AAE of 5, the mean for all missions. For the three
272 ATom missions, AAE values ranged from 2.5 to 8.6 (10th and 90th percentile) and the mean AAE was similar for
273 ATom-2 and 3, but higher for ATom-4 (Table 1). No geographical dependence for AAE was observed, but
274 higher AAE values were always found at high altitude or near the surface. The cause for variability in AAEs is
275 not clear but adds uncertainty to model predictions of radiative effect, which we include in the overall estimated
276 uncertainty.

277

278 A summary of the radiative calculations is shown in Figure 2, where we compare averages for each ATom
279 mission for different groups of data. (DREs of each aerosol component for various latitudes ranges can be found
280 in Table S2). Figure 2a shows the DRE for scattering, and BC and BrC absorption, for data in which the
281 measured WS BrC was above the LOD. For just these data, BrC accounted for 19 to 59% of the carbonaceous
282 aerosol absorption instantaneous forcing, and carbonaceous aerosol absorption DRE offset total light scattering
283 DRE by ~5%. These are periods (BrC>LOD) of sampling in plumes of fairly strong biomass burning influence,
284 as confirmed by the PALMS tracer analysis; for the three ATom missions when BrC>LOD the median
285 contribution of biomass burning to aerosol mass was 30% and median aerosol mass from biomass burning was
286 $0.24 \mu\text{g m}^{-3}$. This contrasts with periods when BrC<LOD shown in Figure 2b, where the magnitudes of the
287 TOA DRE was much smaller for scattering and absorption (contrast scales in Figure 2a and 2b). Based on the
288 PALMS data, for these periods only 8% of the aerosol mass was from biomass burning and the concentration
289 median was $0.03 \mu\text{g m}^{-3}$ (see bar and whisker plot in Supplemental Material Figure S7). BC concentration
290 followed a similar trend, BC was substantially higher when BrC>LOD (i.e, periods of smoke sampling),
291 especially in ATom-2 (Figure S8).

292

293 The average DRE for each mission was also calculated. Figure 2c shows the mean instantaneous DRE at TOA
294 that includes all data, and where BrC < LOD was set to $\frac{1}{2}$ LOD. The ratio of averaged DRE due to BrC was
295 44% of the averaged total light absorption by carbonaceous aerosols among three ATom missions. The mission
296 average was 38% when BrC set equal to 0 for BrC<LOD, (not plotted). The mean results are similar to those

297 periods of BrC>LOD (Figure 2a) since the mean is dominated by the higher magnitude values. Figure 2d gives
298 the DRE results for smoke detected in just the mid-tropical Atlantic, and Table S2 summarizes results from
299 other latitude ranges. These data show that the BrC contribution can be substantial, but with significant
300 variation, ranging from 21% to 59% of the total carbonaceous absorption DRE for the three ATom missions.

301

302 The fraction of carbonaceous aerosol DRE due to BrC for these data are similar to or surpasses the high end of
303 the range reported by other studies [*Feng et al.*, 2013; *Jo et al.*, 2016; *P Lin et al.*, 2015; *Saleh et al.*, 2014;
304 *Wang et al.*, 2016; *A Zhang et al.*, 2020]. A possible reason is the models are truly global averages, whereas this
305 is data only from where the aircraft sampled. Another possible reason is the sensitivity of DRE to the vertical
306 distribution of BrC and BC, which most modeling studies may not correctly simulate. Throughout this study,
307 BC was mainly found from near the surface to mid altitudes, whereas BrC was observed to decrease less slowly
308 with altitude compared to BC, resulting in an increasing of BrC/BC with altitude (Figure S9), as has been seen
309 in continental aerosols [*Liu et al.*, 2014].

310

311 The approach used to investigate BrC based on dissolving aerosol in a solvent and measuring the molecular
312 chromophores exclusive of BC generally has higher sensitivity than instrumentation that measures aerosol light
313 absorption without altering the particle, such as the multi-wavelength photo-acoustic measurement. Even so, the
314 majority of samples in the remote atmosphere were below detection limit using the solvent method. However,
315 measuring dissolved chromophores and then estimating aerosol optical effects introduces uncertainty, as
316 discussed in the Methods section. Sensitivity tests indicate there is nearly a 1:1 correspondence between the
317 change in BrC absorption coefficient and its DRE, implying the uncertainty in BrC TOA DRE is roughly \pm
318 45%, similar to the overall BrC absorption coefficient uncertainty at 365nm. The use of a constant BrC AAE of
319 5, based on the average of all ATOM data, also adds uncertainty to the DRE; the mean DRE due to BrC
320 increases by about 10% for a BrC AAE of 3 instead of 5 and decreases by about 30% for an AAE of 7.
321 Combining these uncertainties, we estimate the overall uncertainty in BrC DRE is roughly 50%. Assuming the
322 uncertainty of DRE due to BC is significantly smaller, the fraction of BrC DRE to total carbonaceous DRE is
323 estimated to be 7 to 23% for ATom-2, 45 to 48% for ATom-3, and 39 to 47% for ATom-4 (range for setting
324 BrC below LOD to zero or $\frac{1}{2}$ LOD) with $\pm 24\%$ uncertainty.

325

326 In summary, the smoldering combustion of wildfires is known to be a significant source of BrC. We find on a
327 global scale, based on the regions measured during ATom-2, 3 and 4 deployments (Jan./Feb., Sept./Oct.,

328 Apr./May), that measurable amounts of BrC were associated with tracers of smoke such as BC, potassium, and
329 PALMS single particle composition. Such smoke contained variable amounts of BrC, which was often detected
330 great distances from the burning regions (greater than 10,000 km), persisting for more than 3 days following
331 emissions. This BrC made a significant contribution to the overall absorption by carbonaceous aerosols and the
332 top of atmospheric direct radiative effect, however the spatial distribution of the BrC forcing was highly
333 heterogeneous.

334

335

336

337 **Acknowledgements:**

338 Research by Georgia Tech was supported by the National Aeronautics and Space Administration's under grant
339 NNX15AT90G and UNH by grant NNX15AG62A. The authors thank all pilots and crew of NASA DC-8 for
340 their role in obtaining the data. We also thank to Dr. Bernadett Weinzierl and her group for the contribution of
341 the cloud data.

342

343 **Data Availability:**

344 The ATom data are available as described by in *Wofsy et al.* [2018], and may also be accessed at
345 <https://doi.org/10.3334/ORNLDAAAC/1581>. More detailed data (BrC and WSOC raw data) can be provided by
346 contacting with the corresponding author.

347

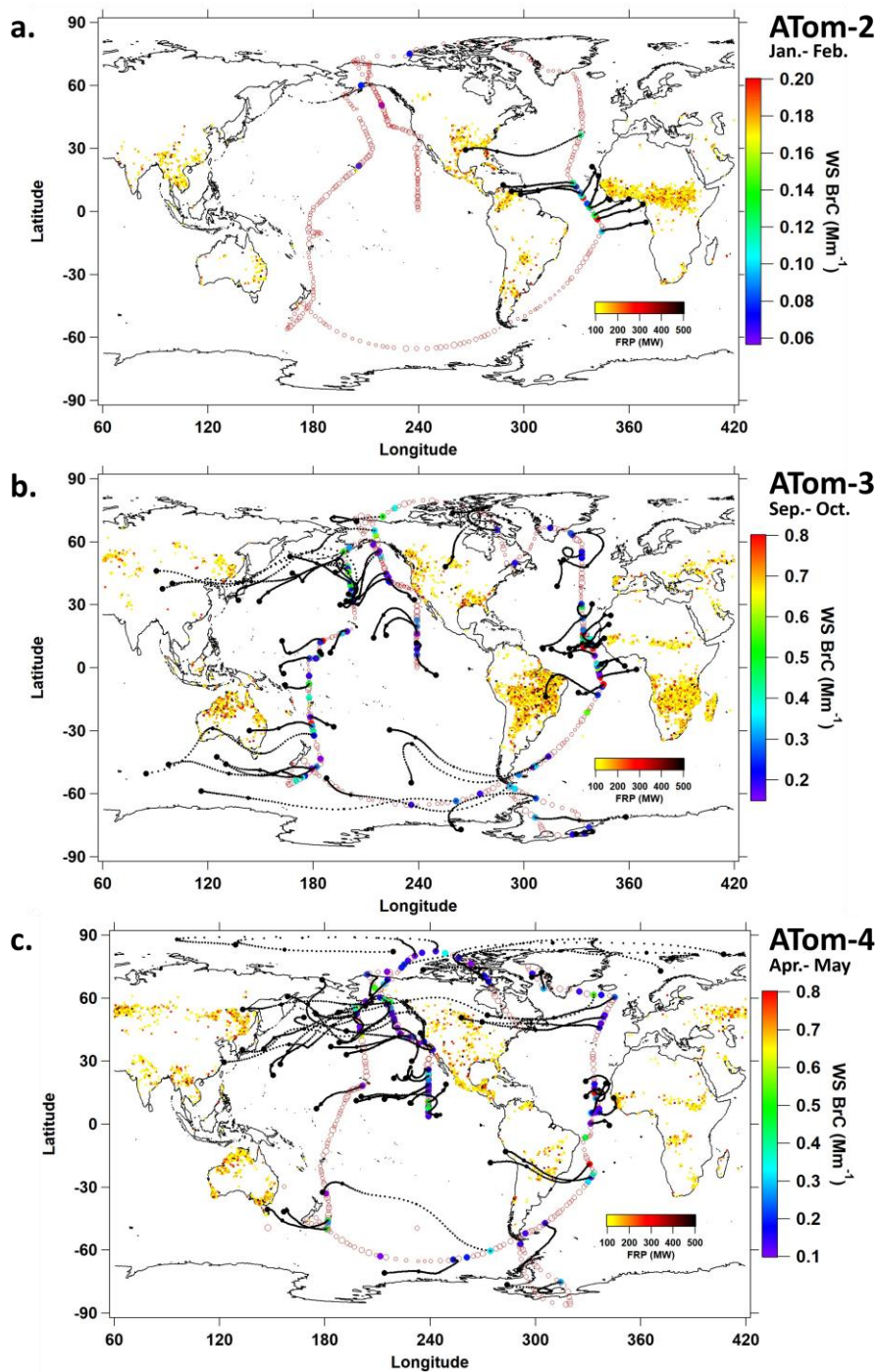
348 **References**

- 349 Adler, G., et al. (2019), Evidence in biomass burning smoke for a light-absorbing aerosol with properties
 350 intermediate between brown and black carbon, *Aerosol Science and Technology*, 53(9), 976-989,
 351 doi:10.1080/02786826.2019.1617832.
- 352 Andrews, E., et al. (2006), Comparison of methods for deriving aerosol asymmetry parameter, *Journal of*
 353 *Geophysical Research: Atmospheres*, 111(D5), doi:10.1029/2004jd005734.
- 354 Bellouin, N., O. Boucher, J. Haywood, and M. S. Reddy (2005), Global estimate of aerosol direct radiative
 355 forcing from satellite measurements, *Nature*, 438(7071), 1138-1141, doi:10.1038/nature04348.
- 356 Bond, T. C., and R. W. Bergstrom (2006), Light Absorption by Carbonaceous Particles: An Investigative
 357 Review, *Aerosol Science and Technology*, 40(1), 27-67, doi:10.1080/02786820500421521.
- 358 Brock, C. A., et al. (2019), Aerosol size distributions during the Atmospheric Tomography Mission (ATom):
 359 methods, uncertainties, and data products, *Atmos. Meas. Tech.*, 12(6), 3081-3099, doi:10.5194/amt-12-
 360 3081-2019.
- 361 Chakrabarty, R. K., et al. (2016), Brown carbon aerosols from burning of boreal peatlands: microphysical
 362 properties, emission factors, and implications for direct radiative forcing, *Atmos. Chem. Phys.*, 16(5), 3033-
 363 3040, doi:10.5194/acp-16-3033-2016.
- 364 Chen, Y., and T. C. Bond (2010), Light absorption by organic carbon from wood combustion, *Atmos. Chem.*
 365 *Phys.*, 10(4), 1773-1787, doi:10.5194/acp-10-1773-2010.
- 366 Chýlek, P., and J. A. Coakley (1974), Aerosols and Climate, *Science*, 183(4120), 75,
 367 doi:10.1126/science.183.4120.75.
- 368 Claeys, M., R. Vermeylen, F. Yasmeeen, Y. Gómez-González, X. Chi, W. Maenhaut, T. Mészáros, and I. Salma
 369 (2012), Chemical characterisation of humic-like substances from urban, rural and tropical biomass burning
 370 environments using liquid chromatography with UV/vis photodiode array detection and electrospray
 371 ionisation mass spectrometry, *Environmental Chemistry*, 9(3), 273-284.
- 372 Cooke, W. F., and J. J. N. Wilson (1996), A global black carbon aerosol model, *Journal of Geophysical*
 373 *Research: Atmospheres*, 101(D14), 19395-19409, doi:10.1029/96JD00671.
- 374 Desyaterik, Y., Y. Sun, X. Shen, T. Lee, X. Wang, T. Wang, and J. L. Collett Jr (2013), Speciation of “brown”
 375 carbon in cloud water impacted by agricultural biomass burning in eastern China, *Journal of Geophysical*
 376 *Research: Atmospheres*, 118(13), 7389-7399, doi:10.1002/jgrd.50561.
- 377 Di Lorenzo, R. A., and C. J. Young (2016), Size separation method for absorption characterization in brown
 378 carbon: Application to an aged biomass burning sample, *Geophysical Research Letters*, 43(1), 458-465,
 379 doi:10.1002/2015GL066954.
- 380 Echalar, F., A. Gaudichet, H. Cachier, and P. Artaxo (1995), Aerosol emissions by tropical forest and savanna
 381 biomass burning: Characteristic trace elements and fluxes, *Geophysical Research Letters*, 22(22), 3039-
 382 3042, doi:10.1029/95GL03170.
- 383 Feng, Y., V. Ramanathan, and V. R. Kotamarthi (2013), Brown carbon: a significant atmospheric absorber of
 384 solar radiation?, *Atmos. Chem. Phys.*, 13(17), 8607-8621, doi:10.5194/acp-13-8607-2013.
- 385 Forrister, H., et al. (2015), Evolution of brown carbon in wildfire plumes, *Geophysical Research Letters*, 42(11),
 386 4623-4630, doi:10.1002/2015GL063897.
- 387 Froyd, K. D., et al. (2019), A new method to quantify mineral dust and other aerosol species from aircraft
 388 platforms using single-particle mass spectrometry, *Atmos. Meas. Tech.*, 12(11), 6209-6239,
 389 doi:10.5194/amt-12-6209-2019.

- 390 Haywood, J., and O. Boucher (2000), Estimates of the direct and indirect radiative forcing due to tropospheric
391 aerosols: A review, *Reviews of Geophysics*, 38(4), 513-543, doi:10.1029/1999rg000078.
- 392 Heald, C. L., D. A. Ridley, J. H. Kroll, S. R. H. Barrett, K. E. Cady-Pereira, M. J. Alvarado, and C. D. Holmes
393 (2014), Contrasting the direct radiative effect and direct radiative forcing of aerosols, *Atmos. Chem. Phys.*,
394 14(11), 5513-5527, doi:10.5194/acp-14-5513-2014.
- 395 Hecobian, A., X. Zhang, M. Zheng, N. Frank, E. S. Edgerton, and R. J. Weber (2010), Water-Soluble Organic
396 Aerosol material and the light-absorption characteristics of aqueous extracts measured over the
397 Southeastern United States, *Atmos. Chem. Phys.*, 10(13), 5965-5977, doi:10.5194/acp-10-5965-2010.
- 398 Hoffer, A., A. Gelencsér, P. Guyon, G. Kiss, O. Schmid, G. P. Frank, P. Artaxo, and M. O. Andreae (2006),
399 Optical properties of humic-like substances (HULIS) in biomass-burning aerosols, *Atmos. Chem. Phys.*,
400 6(11), 3563-3570, doi:10.5194/acp-6-3563-2006.
- 401 Horvath, H. (1993), Atmospheric light absorption—A review, *Atmospheric Environment. Part A. General*
402 *Topics*, 27(3), 293-317, doi:https://doi.org/10.1016/0960-1686(93)90104-7.
- 403 Jo, D. S., R. J. Park, S. Lee, S. W. Kim, and X. Zhang (2016), A global simulation of brown carbon:
404 implications for photochemistry and direct radiative effect, *Atmos. Chem. Phys.*, 16(5), 3413-3432,
405 doi:10.5194/acp-16-3413-2016.
- 406 Koch, D., et al. (2009), Evaluation of black carbon estimations in global aerosol models, *Atmos. Chem. Phys.*,
407 9(22), 9001-9026, doi:10.5194/acp-9-9001-2009.
- 408 Lin, G., J. E. Penner, M. G. Flanner, S. Sillman, L. Xu, and C. Zhou (2014), Radiative forcing of organic aerosol
409 in the atmosphere and on snow: Effects of SOA and brown carbon, *Journal of Geophysical Research:*
410 *Atmospheres*, 119(12), 7453-7476, doi:10.1002/2013JD021186.
- 411 Lin, P., P. K. Aiona, Y. Li, M. Shiraiwa, J. Laskin, S. A. Nizkorodov, and A. Laskin (2016), Molecular
412 Characterization of Brown Carbon in Biomass Burning Aerosol Particles, *Environmental Science &*
413 *Technology*, 50(21), 11815-11824, doi:10.1021/acs.est.6b03024.
- 414 Lin, P., J. Liu, J. E. Shilling, S. M. Kathmann, J. Laskin, and A. Laskin (2015), Molecular characterization of
415 brown carbon (BrC) chromophores in secondary organic aerosol generated from photo-oxidation of toluene,
416 *Physical Chemistry Chemical Physics*, 17(36), 23312-23325, doi:10.1039/C5CP02563J.
- 417 Liu, J., M. Bergin, H. Guo, L. King, N. Kotra, E. Edgerton, and R. J. Weber (2013), Size-resolved
418 measurements of brown carbon in water and methanol extracts and estimates of their contribution to
419 ambient fine-particle light absorption, *Atmos. Chem. Phys.*, 13(24), 12389-12404, doi:10.5194/acp-13-
420 12389-2013.
- 421 Liu, J., et al. (2015), Brown carbon aerosol in the North American continental troposphere: sources, abundance,
422 and radiative forcing, *Atmos. Chem. Phys.*, 15(14), 7841-7858, doi:10.5194/acp-15-7841-2015.
- 423 Liu, J., et al. (2014), Brown carbon in the continental troposphere, *Geophysical Research Letters*, 41(6), 2191-
424 2195, doi:10.1002/2013GL058976.
- 425 Lund, M. T., B. H. Samset, R. B. Skeie, D. Watson-Parris, J. M. Katich, J. P. Schwarz, and B. Weinzierl (2018),
426 Short Black Carbon lifetime inferred from a global set of aircraft observations, *npj Climate and*
427 *Atmospheric Science*, 1(1), 31, doi:10.1038/s41612-018-0040-x.
- 428 McNaughton, C. S., et al. (2007), Results from the DC-8 Inlet Characterization Experiment (DICE): Airborne
429 Versus Surface Sampling of Mineral Dust and Sea Salt Aerosols, *Aerosol Science and Technology*, 41(2),
430 136-159, doi:10.1080/02786820601118406.
- 431 Obregón, M. A., A. Serrano, M. J. Costa, and A. M. Silva (2015), Validation of libRadtran and SBDART
432 models under different aerosol conditions, *IOP Conference Series: Earth and Environmental Science*, 28,
433 012010, doi:10.1088/1755-1315/28/1/012010.

- 434 Phillips, S. M., and G. D. Smith (2017), Spectroscopic comparison of water- and methanol-soluble brown
435 carbon particulate matter, *Aerosol Science and Technology*, *51*(9), 1113-1121,
436 doi:10.1080/02786826.2017.1334109.
- 437 Pio, C. A., M. Legrand, C. A. Alves, T. Oliveira, J. Afonso, A. Caseiro, H. Puxbaum, A. Sanchez-Ochoa, and A.
438 Gelencsér (2008), Chemical composition of atmospheric aerosols during the 2003 summer intense forest
439 fire period, *Atmospheric Environment*, *42*(32), 7530-7543, doi.
- 440 Pio, C. A., et al. (2007), Climatology of aerosol composition (organic versus inorganic) at nonurban sites on a
441 west-east transect across Europe, *Journal of Geophysical Research: Atmospheres*, *112*(D23),
442 doi:10.1029/2006JD008038.
- 443 Prather, M. J., et al. (2017), Global atmospheric chemistry – which air matters, *Atmos. Chem. Phys.*, *17*(14),
444 9081-9102, doi:10.5194/acp-17-9081-2017.
- 445 Ricchiazzi, P., S. Yang, C. Gautier, and D. Sowle (1998), SBDART: A Research and Teaching Software Tool
446 for Plane-Parallel Radiative Transfer in the Earth's Atmosphere, *Bulletin of the American Meteorological*
447 *Society*, *79*(10), 2101-2114, doi:10.1175/1520-0477(1998)079<2101:Saats>2.0.Co;2.
- 448 Rolph, G., A. Stein, and B. Stunder (2017), Real-time Environmental Applications and Display sYstem:
449 READY, *Environmental Modelling & Software*, *95*, 210-228,
450 doi:https://doi.org/10.1016/j.envsoft.2017.06.025.
- 451 Saleh, R., M. Marks, J. Heo, P. J. Adams, N. M. Donahue, and A. L. Robinson (2015), Contribution of brown
452 carbon and lensing to the direct radiative effect of carbonaceous aerosols from biomass and biofuel burning
453 emissions, *Journal of Geophysical Research: Atmospheres*, *120*(19), 10,285-210,296,
454 doi:10.1002/2015JD023697.
- 455 Saleh, R., et al. (2014), Brownness of organics in aerosols from biomass burning linked to their black carbon
456 content, *Nature Geoscience*, *7*, 647, doi:10.1038/ngeo2220
457 <https://www.nature.com/articles/ngeo2220#supplementary-information>.
- 458 Satish, R., and N. Rastogi (2019), On the Use of Brown Carbon Spectra as a Tool to Understand Their Broader
459 Composition and Characteristics: A Case Study from Crop-residue Burning Samples, *ACS Omega*, *4*(1),
460 1847-1853, doi:10.1021/acsomega.8b02637.
- 461 Schill, G. P., et al. (2020), Widespread biomass burning smoke throughout the remote troposphere, *Nature*
462 *Geoscience*, *Accepted*, doi:10.1038/s41561-020-0586-1.
- 463 Schroeder, W., E. Prins, L. Giglio, I. Csizsar, C. Schmidt, J. Morissette, and D. Morton (2008), Validation of
464 GOES and MODIS active fire detection products using ASTER and ETM+ data, *Remote Sensing of*
465 *Environment*, *112*(5), 2711-2726, doi:<https://doi.org/10.1016/j.rse.2008.01.005>.
- 466 Schuster, G. L., O. Dubovik, A. Arola, T. F. Eck, and B. N. Holben (2016), Remote sensing of soot carbon –
467 Part 2: Understanding the absorption Ångström exponent, *Atmos. Chem. Phys.*, *16*(3), 1587-1602,
468 doi:10.5194/acp-16-1587-2016.
- 469 Schwarz, J. P., et al. (2008), Coatings and their enhancement of black carbon light absorption in the tropical
470 atmosphere, *Journal of Geophysical Research: Atmospheres*, *113*(D3), doi:10.1029/2007JD009042.
- 471 Shetty, N. J., A. Pandey, S. Baker, W. M. Hao, and R. K. Chakrabarty (2019), Measuring light absorption by
472 freshly emitted organic aerosols: optical artifacts in traditional solvent-extraction-based methods, *Atmos.*
473 *Chem. Phys.*, *19*(13), 8817-8830, doi:10.5194/acp-19-8817-2019.
- 474 Sokolik, I. N., and O. B. Toon (1999), Incorporation of mineralogical composition into models of the radiative
475 properties of mineral aerosol from UV to IR wavelengths, *Journal of Geophysical Research: Atmospheres*,
476 *104*(D8), 9423-9444, doi:10.1029/1998JD200048.
- 477 Stein, A. F., R. R. Draxler, G. D. Rolph, B. J. B. Stunder, M. D. Cohen, and F. Ngan (2015), NOAA's
478 HYSPLIT Atmospheric Transport and Dispersion Modeling System, *Bulletin of the American*
479 *Meteorological Society*, *96*(12), 2059-2077, doi:10.1175/BAMS-D-14-00110.1.

- 480 Wang, X., C. L. Heald, J. Liu, R. J. Weber, P. Campuzano-Jost, J. L. Jimenez, J. P. Schwarz, and A. E. Perring
481 (2018), Exploring the observational constraints on the simulation of brown carbon, *Atmos. Chem. Phys.*,
482 *18*(2), 635-653, doi:10.5194/acp-18-635-2018.
- 483 Wang, X., C. L. Heald, A. J. Sedlacek, S. S. de Sá, S. T. Martin, M. L. Alexander, T. B. Watson, A. C. Aiken, S.
484 R. Springston, and P. Artaxo (2016), Deriving brown carbon from multiwavelength absorption
485 measurements: method and application to AERONET and Aethalometer observations, *Atmos. Chem. Phys.*,
486 *16*(19), 12733-12752, doi:10.5194/acp-16-12733-2016.
- 487 Washenfelder, R. A., et al. (2015), Biomass burning dominates brown carbon absorption in the rural
488 southeastern United States, *Geophysical Research Letters*, *42*(2), 653-664, doi:10.1002/2014GL062444.
- 489 Wofsy, S. C., et al. (2018), ATom: Merged Atmospheric Chemistry, Trace Gases, and Aerosols, edited, ORNL
490 Distributed Active Archive Center, doi:10.3334/ornl daac/1581.
- 491 Wong, J. P. S., A. Nenes, and R. J. Weber (2017), Changes in Light Absorptivity of Molecular Weight
492 Separated Brown Carbon Due to Photolytic Aging, *Environmental Science & Technology*, *51*(15), 8414-
493 8421, doi:10.1021/acs.est.7b01739.
- 494 Wong, J. P. S., M. Tsagkaraki, I. Tsiotra, N. Mihalopoulos, K. Violaki, M. Kanakidou, J. Sciare, A. Nenes, and
495 R. J. Weber (2019), Atmospheric evolution of molecular-weight-separated brown carbon from biomass
496 burning, *Atmos. Chem. Phys.*, *19*(11), 7319-7334, doi:10.5194/acp-19-7319-2019.
- 497 Wooster, M. J., G. Roberts, G. L. W. Perry, and Y. J. Kaufman (2005), Retrieval of biomass combustion rates
498 and totals from fire radiative power observations: FRP derivation and calibration relationships between
499 biomass consumption and fire radiative energy release, *Journal of Geophysical Research: Atmospheres*,
500 *110*(D24), doi:10.1029/2005JD006318.
- 501 Zhang, A., Y. Wang, Y. Zhang, R. J. Weber, Y. Song, Z. Ke, and Y. Zou (2020), Modeling the global radiative
502 effect of brown carbon: a potentially larger heating source in the tropical free troposphere than black
503 carbon, *Atmos. Chem. Phys.*, *20*(4), 1901-1920, doi:10.5194/acp-20-1901-2020.
- 504 Zhang, X., A. Hecobian, M. Zheng, N. H. Frank, and R. J. Weber (2010), Biomass burning impact on PM_{2.5}
505 over the southeastern US during 2007: integrating chemically speciated FRM filter measurements, MODIS
506 fire counts and PMF analysis, *Atmos. Chem. Phys.*, *10*(14), 6839-6853, doi:10.5194/acp-10-6839-2010.
- 507 Zhang, X., Y.-H. Lin, J. D. Surratt, and R. J. Weber (2013), Sources, Composition and Absorption Ångström
508 Exponent of Light-absorbing Organic Components in Aerosol Extracts from the Los Angeles Basin,
509 *Environmental Science & Technology*, *47*(8), 3685-3693, doi:10.1021/es305047b.
- 510 Zhang, Y., et al. (2017), Top-of-atmosphere radiative forcing affected by brown carbon in the upper
511 troposphere, *Nature Geoscience*, *10*, 486, doi:10.1038/ngeo2960.
- 512
- 513



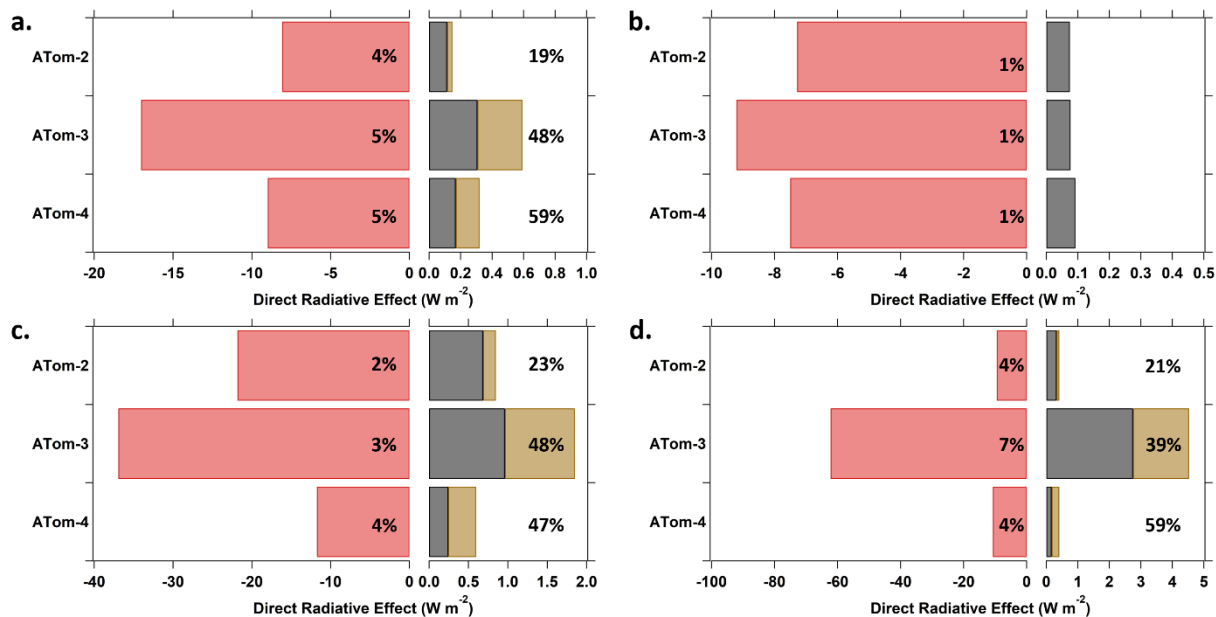
515

516 **Figure 1.** Water-soluble (WS) BrC (Absorption coefficient at 365 nm) global distribution measured in ATom-2
517 (a), ATom-3 (b), and ATom-4 (c). Filled circles are colored by the magnitude of WS BrC for data above the
518 LOD and open circles represent data below the LOD, sized by relative magnitude. Fire dots with greater than
519 100 MW fire radiative power (FRP) are colored by FRP magnitude in all plots. HYSPLIT air mass back
520 trajectories are shown for up to 72 hours, where black dots indicate locations every 24 hours.

521

522

523
524
525
526



527
528

529 **Figure 2.** Instantaneous clear-sky DRE at the top of atmosphere (TOA) computed with ATom data (a) for the
530 average of each ATom mission when BrC data are above LOD, (b) average of each ATom mission when BrC
531 data are below LOD, (c) global average of each ATom mission for all data with BrC < LOD set to ½ LOD, and
532 (d) just for data in the mid-Atlantic (see Figure 1). The percentages shown in the scattering bar are the fraction
533 of DRE due to carbonaceous aerosol absorption relative to scattering, $Abs(BC+BrC)/Scat.$, and the percentages
534 shown to the right of the bar are the fraction of DRE due to BrC of all carbonaceous absorbing species,
535 $Abs(BrC)/Abs(BC+BrC)$. Note the scale changes at the point zero since aerosol scattering dominates TOA DRE
536 in remote regions.

537
538

539

540 **Table 1.** ATom data summary. BrC absorption data are for only water-soluble species.

	ATom-2	ATom-3	ATom-4
Deployment dates	26 Jan. to 21 Feb. 2017	8 Sept. to 27 Oct. 2017	24 Apr. to 21 May 2018
Number of filters analyzed	323	380	362
BrC LOD, Mm^{-1}	0.05	0.15	0.10
% of filters above LOD	5.1	28.4	27.3
BrC Mean: Data below LOD set to $\frac{1}{2}$ LOD, Mm^{-1}	0.003	0.172	0.099
BrC Median: No adjustment for below LOD (Median for only data above LOD), Mm^{-1}	-0.001 (0.098)	0.066 (0.276)	0.042 (0.172)
Water-soluble BrC to Total BrC Ratio	N.A.	57%±17%	50%±16%
AAE mean: wavelength ranges from 300 to 500 nm	4.1	4.3	6.5
Number of FIRMS identified fire counts with FRP greater than 100 MW globally	13,905	33,070	18,408
BrC mean DRE, (BrC set to zero for data below LOD), W m^{-2}	+0.033 (+0.01)	+0.29 (+0.25)	+0.15 (+0.11)
BC mean DRE, W m^{-2}	+0.11	+0.31	+0.17
Scattering Mean DRE, W m^{-2}	-8.07	-17.02	-8.99

541

542 To estimate corresponding aerosol absorption coefficients, liquid absorption coefficients should be multiplied by
543 a factor of 1.8 to 2 (see text). The Direct Radiative Effect (DRE) was based on water-soluble BrC multiplied by
544 a factor of 4 to account for conversion of liquid measurement of chromophores to particle absorption and
545 convert water-soluble BrC to total BrC absorption (see WS BrC/Total BrC row above).

546

547

548